Pergamon

Int. J. Heat Mass Transfer. Vol. 37, No. 10, pp. 1455–1464, 1994

0017-9310/94 $7.00 + 0.00

0017-9310(93)E0040-N

Occurrence and development of double-diffusive convection during solidification of a binary system

TATSUO NISHIMURA and TSUTOMU IMOTO
Department of Mechanical Engineering, Yamaguchi University, Ube 755, Japan

and

HISASHI MIYASHITA
Department of Materials Science and Engineering, Toyama University, Toyama 930, Japan

(*Received* 8 *July* 1993 *and in final form* 18 *November* 1993)

Abstract—This paper describes the occurrence and development of double-diffusive convection in the liquid phase during solidification of NH_4Cl–H_2O system in a confined cavity with lateral cooling. Multiple point measurements of concentration show a step change in the vertical direction, and temperature visualizations reveal an S-shaped profile of isotherms, which indicate the existence of time-dependent horizontally-stacked roll cells separated by diffusive interfaces. The cells are generated in a sequential fashion, rather than simultaneously and the thickness of each cell increases with progression of solidification. The concentration in each cell is found to remain nearly constant, except for the initial development of cells. Convection within each cell is largely controlled by the temperature field, and diffusion is dominant in the diffusive interface between two cells due to the solute field with a vertical concentration gradient. The fluid in the diffusive interface is initially stagnant, but the interface changes into a new cell under a certain condition. The criteria for cell generation are determined by the buoyancy ratio and the thermal Rayleigh number in the diffusive interface.

1. INTRODUCTION

NATURAL convective flows have been known for some time to have an important influence on solidification process. In recent years, experimental and numerical treatments of solidification in a binary system have been stimulated by materials processing such as semiconductor crystal growth and the casting of metallic alloys. Although there are several important transport phenomena during solidification, as reviewed by Viskanta [1], we focus on double-diffusive convection which is naturally present in the melt of a binary system. As could be observed from a phase diagram of multicomponent substances, the composition of the resulting solid is generally different from that of the melt when a melt of two or more component solidifies. Therefore, heat and mass transfer occurs simultaneously in the melt, which leads to a complex fluid motion called double-diffusive convection.

The importance of double-diffusive convection during solidification has been first identified in geophysics and metallurgy, and the experimental studies have provided qualitative features based on flow visualizations such as shadowgraph and dyeing techniques (Chen and Turner [2], Szekely and Jassal [3]), e.g. salt fingers and sharp diffusive interfaces. More recently, multiple point measurements of temperature and concentration fields during solidification of aqueous solutions have been performed by heat-transfer investigators (Beckermann and Viskanta (NH_4Cl–H_2O) [4], Christenson and Incropera (NH_4Ci–H_2O) [5], Okada *et al.* ($NaCl$–H_2O) [6] and Nishimura *et al.* (Na_2CO_3–H_2O) [7]). However, there is a further need for detailed velocity, temperature and concentration measurements to understand the role of double-diffusive convection in the solidification process.

Numerical analysis has also come to be used for prediction of solidification of a binary system due to the rapid development of computers. Most of the numerical computations are directed to the horizontal solidification, i.e. Beckermann and Viskanta (NH_4Cl–H_2O) [4], Thompson and Szekely (Na_2CO_3–H_2O) [8], Christenson *et al.* (NH_4Cl–H_2O) [9] and Okada *et al.* ($NaCl$–H_2O) [6], because the solid–liquid interface changes remarkably in the vertical direction by double-diffusive convection, and therefore simple theoretical modelling is difficult. However, the numerical results fail to achieve close quantitative agreement with experimental data for solidification with a mushy zone consisting of a mixed region of liquid and dendritic crystals. Furthermore, the computations have been limited to the initial development of solidification, and time evolution of double-diffusive convection is not evident.

NOMENCLATURE

C	concentration	ΔT	horizontal temperature difference
C_e	concentration at the eutectic point	t	time
C_i	initial concentration	x	vertical coordinate
ΔC	vertical concentration difference	y	horizontal coordinate.
H	height of the enclosure		
L	length of the enclosure	Greek symbols	
N	critical buoyancy ratio	α	thermal diffusivity
Ra_c	critical Rayleigh number defined by equation (4)	β_C	volumetric coefficient with concentration
		β_T	volumetric coefficient with temperature
T	temperature	η	thickness of diffusive interface
T_c	temperature at the cold wall	η^*	vertical scalelength
T_e	temperature at the eutectic point	η_c	critical thickness of diffusive interface
T_i	initial temperature	ν	kinematic viscosity.

Thus, additional experimental and numerical works are required for proper modelling of transport processes of heat and species during solidification. This lack motivated the present experimental investigation.

In order to obtain the detailed information on the development of double-diffusive convection through the solidification process, we performed temperature and flow visualizations using liquid crystals during solidification of an aqueous solution of NH_4Cl–H_2O in a confined cavity with lateral cooling. Temperature and concentration at several positions were also measured by thermocouples and the sample extraction method using microsyringes, respectively. The visualizations and the measurements were conducted simultaneously so that we exactly understand transport processes of time-dependent double-diffusive convection.

2. EXPERIMENTAL APPARATUS AND PROCEDURE

Figure 1 shows a schematic diagram of the experimental apparatus. Solidification of an aqueous ammonium chloride solution was performed in a rectangular test cell with inner dimensions of 37 mm in length, 50 mm in height and 30 mm in width. The test cell was made of acrylic resin, except for the cold wall which consisted of a copper plate. An overflow tube was attached to the test cell in order to eliminate any volume changes in the test cell. A cooling chamber was attached to the rear side of the cold wall, and the wall temperature was maintained at a given cold temperature by refrigeration unit 1. Refrigeration unit 2 was used to control the initial temperature of the aqueous solution. To minimize heat losses, the test cell was insulated with 60 mm of styrofoam on all sides, and, furthermore, the experimental apparatus was placed in a temperature controlled room.

Usually temperatures have been measured by thermocouples in heat transfer experiments, but it may be difficult to deduce the time dependent temperature field in which double-diffusive convection occurs. In fact several investigators (Christenson and Incropera [5] and Okada *et al.* [6]) attempted to obtain temperature fields by use of many thermocouples for solidification of aqueous solutions, but the measurements did not necessarily provide useful information on time dependent double-diffusive processes. We perform temperature visualization using encapsulated liquid crystals suspended in an aqueous solution during solidification, together with multiple point measurements by thermocouples. The liquid crystals used here are a chiral nematic type manufactured by BDH Chemical Ltd. This simple technique has been confirmed to be helpful in interpreting time dependent

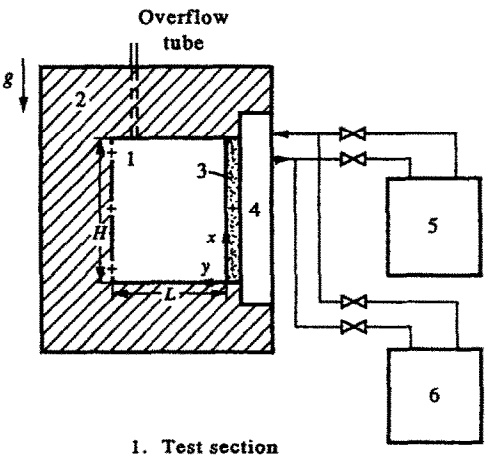

FIG. 1. Schematic diagram of experimental apparatus.

natural convection and freezing of water (Nishimura *et al.* [10]). Furthermore, this liquid crystal was found to be stable even in aqueous solutions of different types of salts and was used to examine double-diffusive convection (Nishimura *et al.* [11, 12]). Also it should be noted that the flow field is observed by the motion of liquid crystals particles. The experimental procedure is mentioned in these references.

Although there are some techniques for species concentration measurements in flowing aqueous solutions, time-dependent concentration measurements are very rare in the solidification process. In this experiment, the variation of concentration with time at several positions in the test cell was determined by the sample extraction method using microsyringes. For this purpose, eight holes of 0.5 mm in diameter in the vertical direction were made at the back wall of the test cell. Through the hole, the aqueous solution of 0.05 ml was extracted by a microsyringe and its refractive index was read through a refractometer at 25°C. The liquid in the overflow tube supplies the reduction of the liquid in the test cell due to the concentration measurement. This procedure was repeated at a position three times and each refractive index was averaged. The deviation from the average values was within $\pm 5\%$. Since the needle of the microsyringe was inserted slowly and normal to the flow direction, the disturbance of the flow, temperature and concentration fields due to sample extraction was negligible.

The equilibrium phase for aqueous ammonium chloride shown in Fig. 2 has an eutectic temperature and concentration (NH_4Cl mass fraction) of $T_e = -15.4$°C and $C_e = 19.7$ wt%, respectively. A solution with composition less than the eutectic value releases more dense fluid during solidification (sub-eutectic growth), while a solution with greater than the eutectic value releases less dense fluid (super-eutectic growth).

3. RESULTS AND DISCUSSION

Figure 3 shows temperature variation with time at the mid-height of the insulated wall opposite to the cold wall for several initial concentrations. The cold wall temperature variation is also shown for $C_i = 25$ wt% for reference, since the cold wall temperatures for all experiments are the same. The initial temperature is 25°C for any case. The insulated wall temperature for $C_i = 19.7$ wt% of the eutectic falls most rapidly, because heat transfer is the only transport process. On the contrary, for both sub-eutectic and super-eutectic cases, the temperature drop is retarded and a small peak appears. This behavior is due to double-diffusive effects as described below. In the following section we present the details of transport processes for super-eutectic growth of 25 wt%.

Figure 4 shows schematic solidification morphology and flow patterns in the fluid region for super-eutectic growth, i.e. $C_i = 25$ wt%, $T_i = 25$°C and $T_C = -14.4$°C. Under this experimental condition, dendritic crystals of NH_4Cl are only formed and a mushy zone comprises a mixed region of liquid and crystals, since the cold wall is above the eutectic temperature $T_e = -15.4$°C. Direct photographs of solidification morphology and flow patterns in the liquid region are shown in Fig. 10.

In the supercooling process, heat transfer is the only transport process and a large clockwise rotating

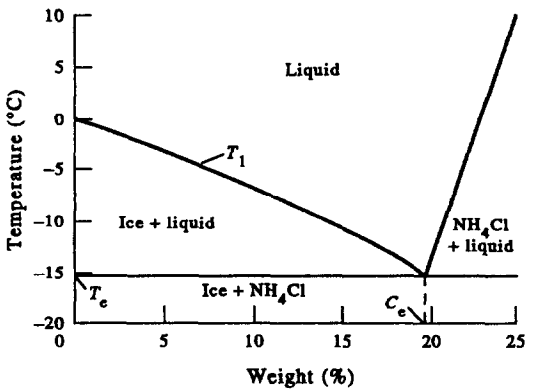

FIG. 2. Equilibrium phase diagram for NH_4Cl–H_2O system.

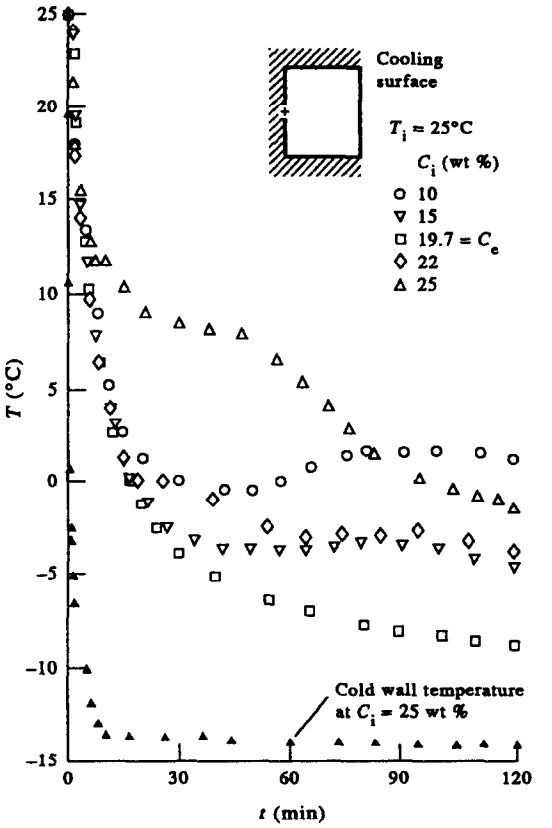

FIG. 3. Temperature histories during solidification at the insulated wall: effect of initial concentration.

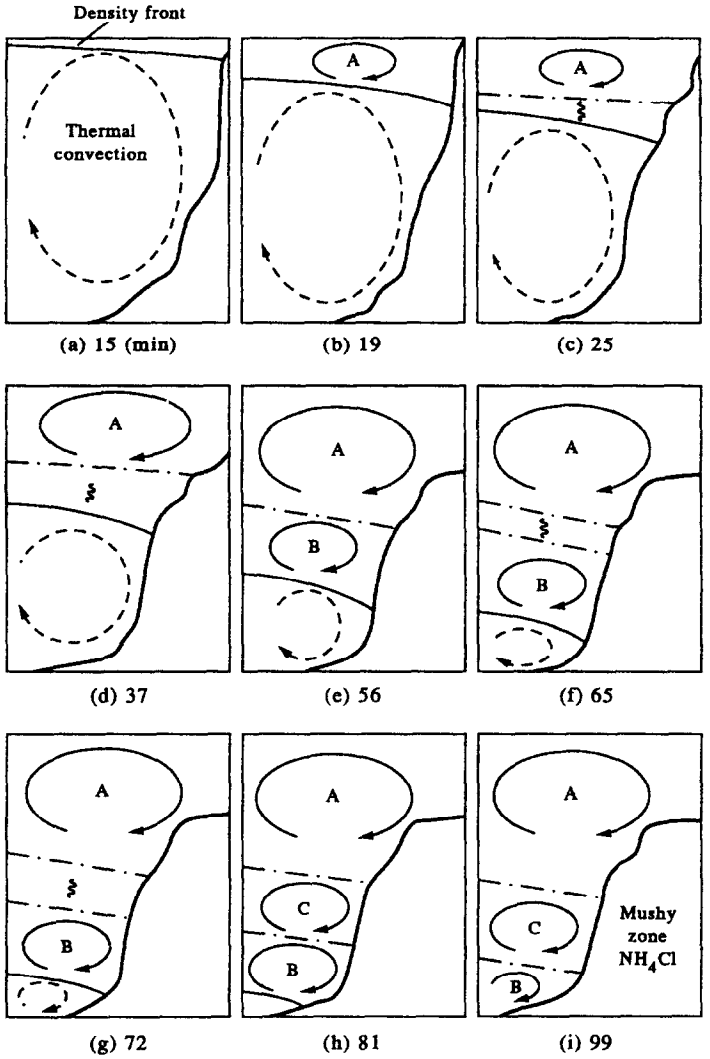

FIG. 4. Time evolution of solidification morphology and flow patterns for a super-eutectic growth ($C_i = 25$ wt%, $T_i = 25°C$, $T_e = -14.4°C$).

circulation is observed due to thermal convection. At the beginning of the crystal growth process, crystallization occurs at the several positions along the cold wall. A water-rich fluid is released and therefore rises along the crystal front, in spite of the fact that the fluid is cooled down. This is solutal convection. Namely, downward thermal boundary layer flow and upward solutal boundary layer flow coexist near the crystals. It should be also noted that some crystals detach from the cold wall and accumulate at the bottom of the cavity.

As the cooling progresses, a cold water-rich fluid, released by the crystal formation, rises up through the mushy zone and accumulates at the top of the cavity, causing thermally unstable and solutally stable conditions. Therefore, there is a sharp density front between the dilute fluid layer and the initially homogeneous fluid layer, marking the beginning of the filling-box process with double-diffusive effects, i.e. compositional stratification (see Fig. 4(a)). The fluid below the density front is dominated by thermal convection, but this is damped by the compositional stratification in the fluid above the density front, which was confirmed by the behavior of particle paths and isotherms revealed by liquid crystals suspended in the solution. When the upper layer above the density front reaches a certain thickness, a clockwise circulation is formed inside the layer, which is called cell A (see Fig. 4(b)).

With progression of solidification, the position of the density front moves downwards and double-diffusive cells are formed above the density front (see Figs. 4(c)–(i)). They finally consist of three horizontally-stacked clockwise circulations in this experiment, i.e. cells A, B and C. Features of double-diffusive cells during solidification are described as follows.

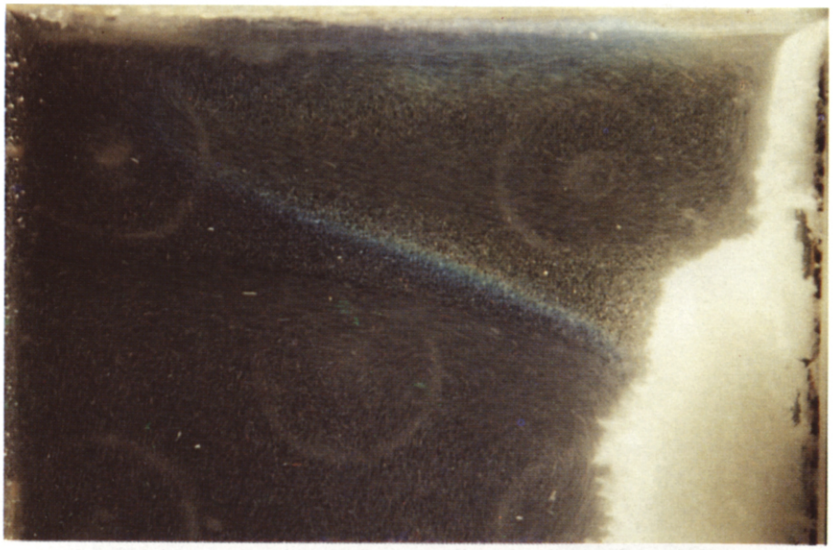

25 (min)

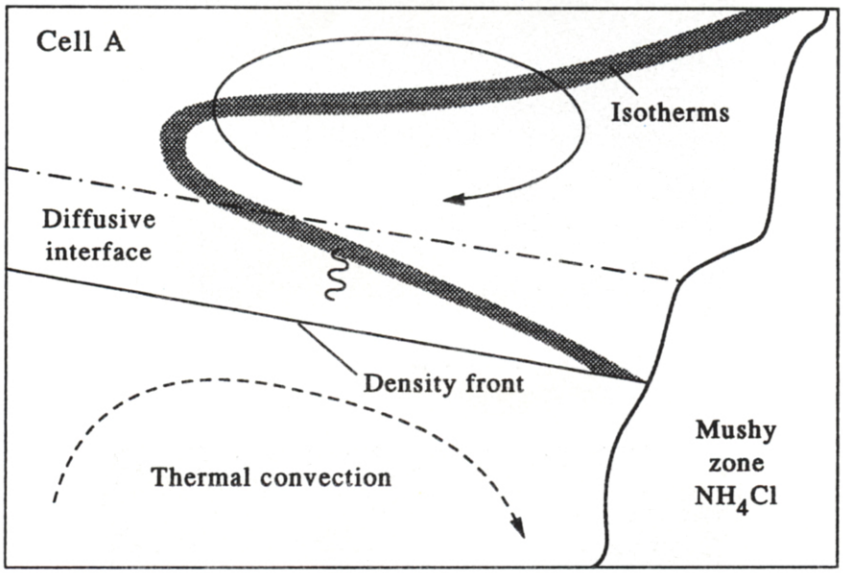

FIG. 5. Visualization photograph of flow and temperature fields above the density front.

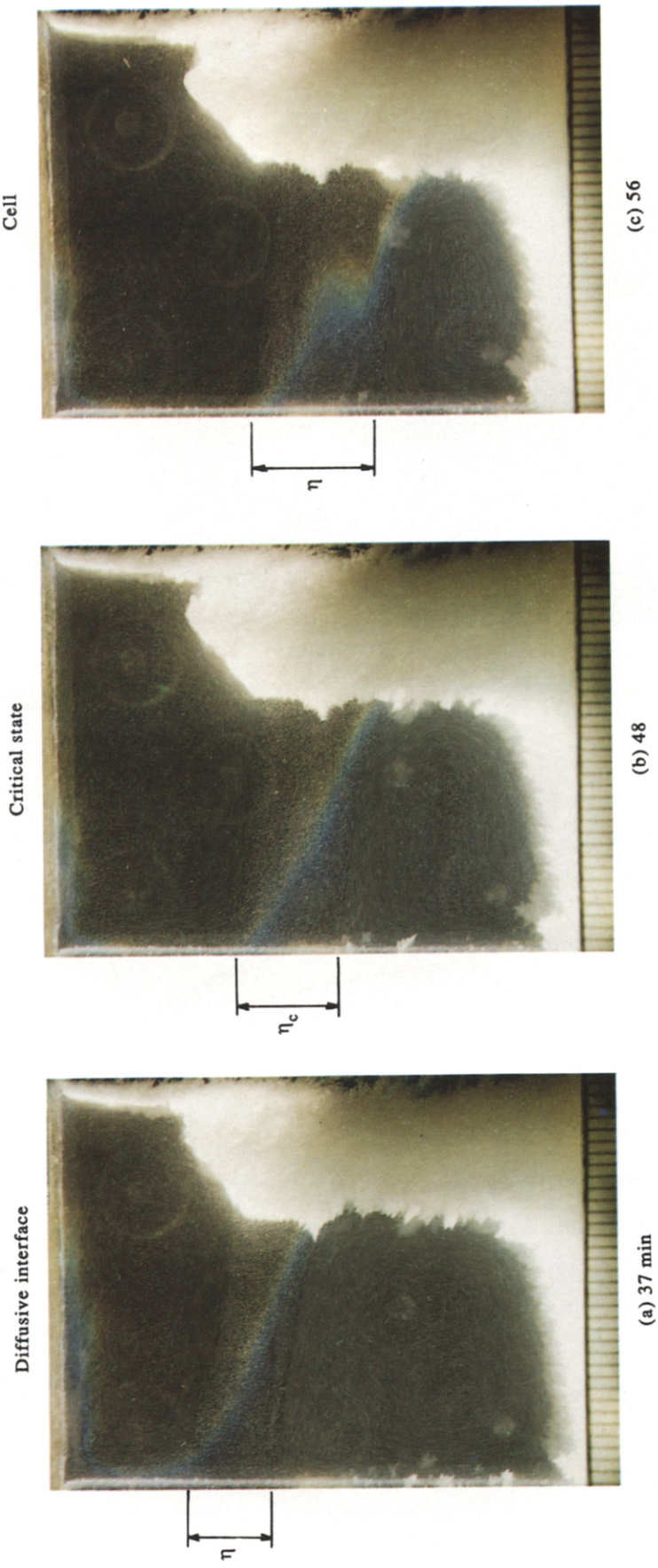

FIG. 10. Generation of a new cell.

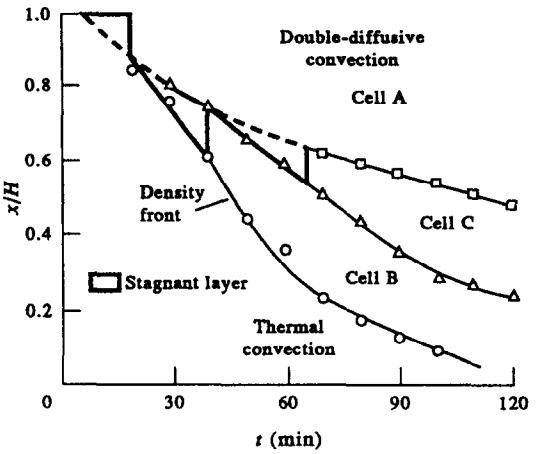

FIG. 6. Development of a multiple cell structure during solidification.

A thin diffusive interface exists between cells and each cell behaves as a separate cell. These cells are generated in a sequential fashion, rather than simultaneously, along the boundaries between existing cells, i.e. diffusive interfaces. The diffusive interface which changes into a new cell is initially stagnant. As the thickness of the interface reaches a certain size, the fluid in the interface begins to rotate in the same direction as old cells. There thus exists a critical condition for the generation of cells.

Figure 5 shows a representative photograph of the corresponding flow and temperature fields above the density front, which is revealed by liquid crystals. The particle paths of liquid crystals enable us to estimate the magnitude of velocity. For example, the horizontal velocity just below the density front in the thermal convection-dominated region is about 3.5 cm min^{-1}, which is comparable with the result in the boundary layer regime for thermal convection [13] although the systems are different. The liquid crystals have a working range of -1 to $-3°C$, and the green color approximately indicates the $-2°C$ isotherm. A diffusive interface and cell A exist above the density front. The fluid in the diffusive interface is stagnant and the isotherms revealed by liquid crystals are tilted downwards, while a strong clockwise circulation is observed in cell A and the isotherms are tilted upwards. The same trends are observed in other diffusive interfaces and cells formed with further progression of solidification. Thus it is found that the vertical temperature gradient in diffusive interfaces causes thermally unstable conditions and is opposite to that in cells.

Figure 6 shows the position of the diffusive interfaces at the insulated wall opposite to the cold wall given as a function of time. The density front moves downwards with time due to the release of a water-rich fluid. Each cell is generated from a diffusive interface and then grows up and moves downwards with progressing solidification.

Figure 7 shows the corresponding temperature variations with time at three different positions of the insulated wall. At the initial stages of solidification, temperature falls rapidly from the bottom of the cavity due to thermal convection. However, the trend is reversed and also the temperature drop becomes slow, as the solidification progresses. This behavior is due to the filling-box process with double-diffusive effects from the top of the cavity and is easily identified from the results shown in Figs. 5 and 6. After the density front passes each measuring point, the temperature drop occurs again.

Figure 8 shows the corresponding concentration change with time for several positions in the fluid region. Figure 8(a) is the result in which the measuring point ($x/H = 0.89$ and $y/L = 0.93$) is located in cell A through the solidification process. After the density front passes the measuring point, the concentration rapidly decreases and then becomes nearly constant, $C > C_e$. Figure 8(b) is the result at the measuring point which cells A, B and C pass ($x/H = 0.5$ and $y/L = 0.93$). When the measuring point is located in each cell, the concentrations are constant, but different to each other. However, when the measuring point changes from one cell to other (or passes a diffusive interface), the concentration rapidly decreases. Figure 8(c) shows the result of the measuring point at the lower part of the cavity ($x/H = 0.32$ and $y/L = 0.59$). When cells B and C pass this point, the concentration change is similar to the result of Fig. 8(b). Comparison of Figs. 8(a)–(c) also indicates that the concentration in each cell is nearly constant even if the measuring points are different, and that the compositional strati-

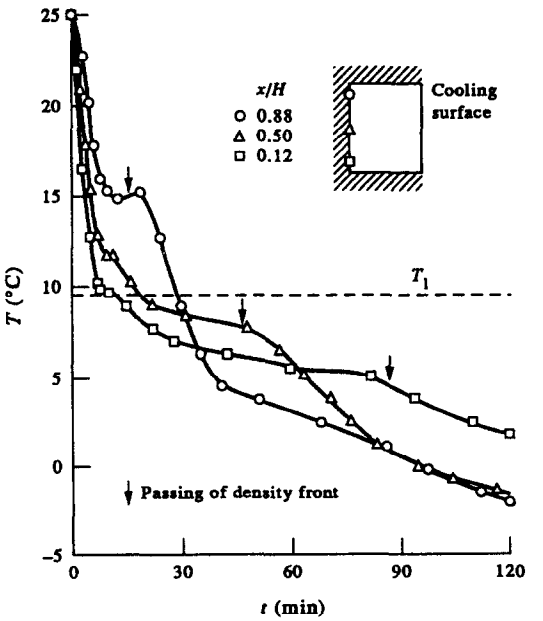

FIG. 7. Temperature histories at different positions of the insulated wall.

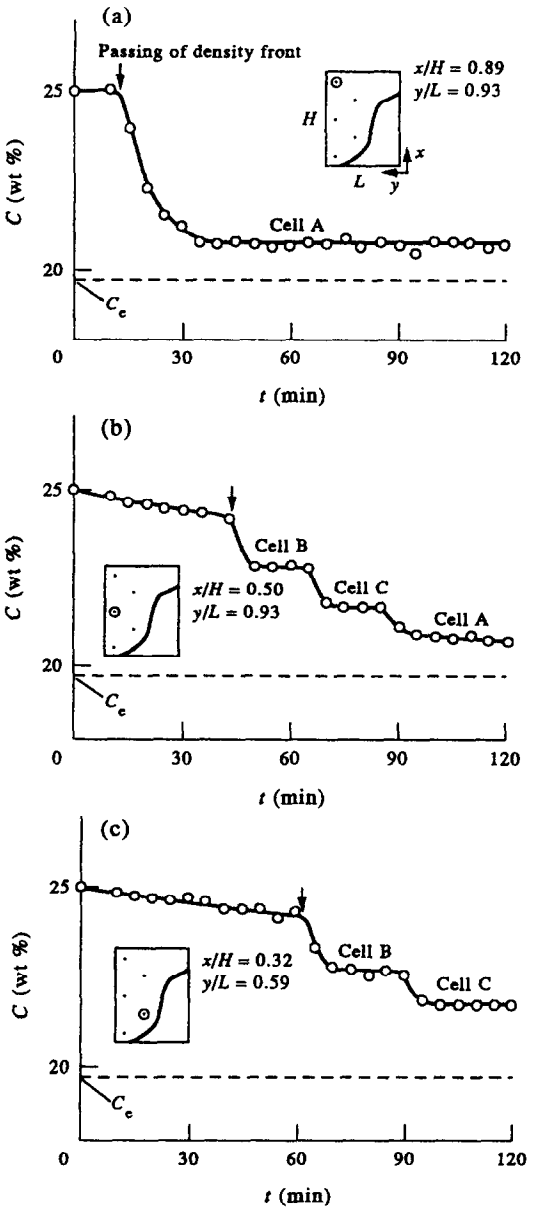

FIG. 8. Concentration histories at different positions in the liquid region.

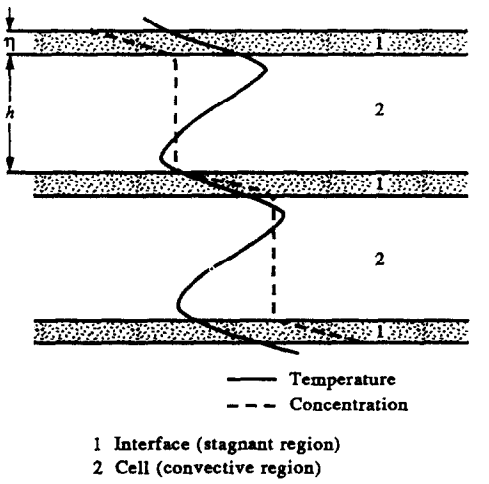

FIG. 9. Typical temperature and concentration profiles in the cells and diffusive interfaces.

fication occurs from the top of the cavity. These results reveal that, within each cell, the solute field is uniform, while solute levels vary quickly across the diffusive interface.

In terms of solidification morphology, the double-diffusive convection patterns have a profound influence (see Figs. 4(a)–(i)). In the early stages of solidification, the shape of the mushy zone is predominantly affected by thermal convection. In the later stages of the experiment, the dendritic crystals are remelted in the upper portion of the cavity and then the solidification is completely terminated. This is because the concentration of the fluid decreases as a result of solidification from the top of the cavity as shown in Fig. 8(a). Higher water concentration results in a lower liquidus temperature according to the phase diagram as shown in Fig. 2. Also the step changes in the horizontal extent of the mushy zone are due to the existence of the horizontally-stacked roll cells described above.

On the basis of the above results, we deduce the structure of horizontally-stacked roll cells. Time-dependent concentration measurements show that, within each cell, the solute field is nearly uniform, while solute levels vary extensively across the interface. The temperature visualizations reveal that the vertical temperature gradient in the diffusive interface causes a thermally unstable condition and is of opposite sign to that in the cell. Combining the profiles of both temperature and concentration, convection within each cell is largely controlled by the temperature field, and diffusion is dominant in the diffusive interface between two cells due to the solute field with a vertical concentration gradient as shown in Fig. 9. There is a clear separation between the cell and the diffusive interface.

Finally we examine the criteria for cell generation during solidification. Figure 10 shows the change from the diffusive interface above the density front to a new cell B, as an example. The cell generation is easily identified by the behavior of particle paths and isotherms revealed by liquid crystals. The left-hand photograph indicates that the fluid in the diffusive interface is still stagnant, while the right-hand photograph shows the state of cell B, and the isotherms are highly deformed by a clockwise rotating circulation. The middle photograph shows a critical state. The diffusive interface thickness gradually increases during the change from a diffusive interface to a new cell and thus is an important factor for the cell generation.

The diffusive interface thickness at the critical state is related to the interaction of the horizontal temperature difference with the vertical solute gradient in the diffusive interface. Because the horizontal temperature difference leads to the generation of cells, i.e. destabilizing force, while the vertical solute gradient maintains a stagnant region, i.e. stabilizing force. The vertical lengthscale corresponding to the diffusive interface thickness is given in terms of the temperature difference and the concentration gradient:

$$\eta^* = \beta_T \Delta T/(\beta_c(-dC/dx)). \quad (1)$$

This implies the distance in which a fluid element can rise in a given vertical solute gradient to neutrally buoyant. For example, the lengthscale increases as the vertical solute gradient decreases. On the basis of the above experimental results (see Fig. 9), the vertical solute gradient in the diffusive interface is approximately represented as follows:

$$dC/dx \sim \Delta C/\eta_c \quad (2)$$

where ΔC is the concentration difference between two cells separated by an aimed diffusive interface.

Equation (1) is thus transformed into equation (3):

$$\eta^* = (1/N)\eta_c \quad (3)$$

where N is the buoyancy ratio $\beta_c \Delta C/\beta_T \Delta T$. If the diffusive interface changes into a single cell rather than multiple cells, the lengthscale η^* is considered to be equal to the diffusive interface thickness η_c. Thus we deduce that the buoyancy ratio has the order of unity at the critical state for the generation of a single cell. Also there exists a critical thermal Rayleigh number beyond which viscous forces are overcome. We estimate experimentally the buoyancy ratio and the thermal Rayleigh number at the critical state. The Rayleigh number is defined by the following equation:

$$Ra_c = g\beta_T \Delta T \eta_c^3/(\nu\alpha) \quad (4)$$

where ΔT is the horizontal temperature difference between the insulated wall and the front of the mushy zone in an aimed diffusive interface. The front temperature of the mushy zone was estimated by the isotherms revealed by liquid crystals (± 0.3°C).

Table 1 shows the buoyancy ratio and the thermal Rayleigh number at the critical state for two experiments which are different in the cold wall temperature. The estimated buoyancy ratio is the order of unity for both the experiments and agrees well with the value predicted by using equation (3). The Rayleigh number is on the order of 10^4 and is near the critical Rayleigh number determined experimentally by Chen *et al.* [14] ($1.5 \times 10^4 \pm 2500$). They studied thermal convection in a salinity gradient due to lateral heating with no solidification. These results confirm that the system is governed by stability criteria analogous to those for double-diffusion between impermeable boundaries without phase change.

Table 1. Physical properties of NH_4Cl-H_2O system and critical values of η_c, N_c and Ra_c for cell generation

T_c	−14.4 [°C]	−28.8 [°C]
β_T	3.8321×10^{-4} [°C^{-1}]	
β_C	2.5679×10^{-3} [wt%$^{-1}$]	
ν	1.3×10^{-6} [m^2 s^{-1}]	
α	1.33×10^{-7} [m^2 s^{-1}]	
η_c	5.17×10^{-3} [m]	3.75×10^{-3} [m]
$(\Delta T)_h$	9.59 [°C]	13.65 [°C]
$(\Delta C)_v$	2.40 [wt%]	2.34 [wt%]
N_c	1.67	1.14
Ra_c	2.88×10^4	1.56×10^4

4. CONCLUSIONS

We performed temperature and flow visualizations during solidification for a NH_4Cl–H_2O system. Temperature and concentration at several positions were simultaneously measured. The structure of time-dependent horizontally-stacked roll cells due to double-diffusive effects were presented.

The cells are generated in a sequential fashion, rather than simultaneously. Although the thickness of each cell increases with progression of solidification, the concentration in each cell remains nearly constant. Convection within each cell is largely controlled by the temperature field, and diffusion is dominant in the diffusive interface between cells due to the solute field with a vertical concentration gradient.

The fluid in the diffusive interface is initially stagnant, but begins to rotate in the same direction as old cells as the thickness of the diffusive interface reaches a certain value. The criteria for cell generation was determined by the buoyancy ratio on the order of unity and the thermal Rayleigh number on the order of 10^4 in the diffusive interface.

Acknowledgement The authors acknowledge with thanks the assistance of graduate student Isamu Takemori in the experiments.

REFERENCES

1. R. Viskanta, Mathematical modeling of transport processes during solidification of binary systems, *JSME Int. J.*, Ser. II **33**, 409–423 (1990).
2. C. F. Chen and J. S. Turner, Crystallization in a double-diffusive system, *J. Geophys. Res.* **85**, 2573–2593 (1980).
3. J. Szekely and A. S. Jassal, An experimental and analytical study of the solidification of a binary dendritic system, *Metal. Trans. B* **9**, 389–398 (1978).
4. C. Beckermann and R. Viskanta, Double-diffusive convection during dendritic solidification of a binary mixture, *Phys. Chem. Hydrodyn.* **10**, 195–213 (1988).
5. M. S. Christenson and F. P. Incropera, Solidification of an aqueous ammonium chloride solution in a rectangular cavity—I. Experimental study, *Int. J. Heat Mass Transfer* **32**, 47–68 (1989).
6. M. Okada, K. Gotoh and M. Murakami, Solidification of an aqueous solution in a rectangular cell with hot and cold vertical walls, *Trans JSME Ser. B* **56**, 1790–1795 (1990).
7. T. Nishimura, M. Fujiwara and H. Miyashita, Double-

diffusive convection during solidification of a binary system, *Trans. JSME Ser. B* **58,** 490–496 (1982) or *Heat Transfer—Jpn. Res.* **21,** 586–600 (1992).
8. M. E. Thompson and J. Szekely, Mathematical and physical modeling of double-diffusive convection of aqueous solutions crystallizing at a vertical wall, *J. Fluid Mech.* **187,** 409–433 (1989).
9. M. S. Christenson, W. D. Bennon and F. P. Incropera, Solidification of an aqueous ammonium chloride solution in a rectangular cavity—II. Comparison of predicted and measured results, *Int. J. Heat Mass Transfer* **32,** 69–79 (1989).
10. T. Nishimura, M. Fujiwara, N. Horie and H. Miyashita, Temperature visualizations by use of liquid crystals of unsteady natural convection during supercooling and freezing of water in an enclosure with lateral cooling, *Int. J. Heat Mass Transfer* **34,** 2663–2668 (1991).
11. T. Nishimura, M. Fujiwara and H. Miyashita, Visualization of temperature fields and double-diffusive convection using liquid crystals in an aqueous solution crystallizing along a vertical wall, *Exp. Fluids* **12,** 245–250 (1992).
12. T. Nishimura, M. Fujiwara and H. Miyashita, Visualization of temperature and flow fields using liquid crystals in the fluid region during various solidification processes. In *Flow Visualization* (Edited by Y. Tanida and H. Miyashiro), Vol. 6, pp. 456–460. Springer-Verlag, Berlin (1992).
13. R. A. W. M. Henkes, Natural convection boundary layers, Ph.D. Thesis, Delft University of Technology (1990).
14. C. F. Chen, D. G. Briggs and R. A. Wirtz, Stability of thermal convection in a salinity gradient due to lateral heating, *Int. J. Heat Mass Transfer* **14,** 57–65 (1971).